Cell

Step-Wise Methylation of Histone H3K9 Positions Heterochromatin at the Nuclear Periphery

Benjamin D. Towbin,[1,2] Cristina González-Aguilera,[3] Ragna Sack,[1] Dimos Gaidatzis,[1] Véronique Kalck,[1] Peter Meister,[1,4] Peter Askjaer,[3] and Susan M. Gasser[1,2,*]
[1]Friedrich Miescher Institute for Biomedical Research, Maulbeerstrasse 66, 4058 Basel, Switzerland
[2]Faculty of Sciences, University of Basel, 4056 Basel, Switzerland
[3]Centro Andaluz de Biología del Desarrollo (CABD), Consejo Superior de Investigaciones Científicas, Universidad Pablo de Olavide, Seville 41013, Spain
[4]Present address: University of Bern, Institute of Cell Biology, Baltzerstrasse 4, 3012 Bern, Switzerland
*Correspondence: susan.gasser@fmi.ch
http://dx.doi.org/10.1016/j.cell.2012.06.051

SUMMARY

The factors that sequester transcriptionally repressed heterochromatin at the nuclear periphery are currently unknown. In a genome-wide RNAi screen, we found that depletion of S-adenosylmethionine (SAM) synthetase reduces histone methylation globally and causes derepression and release of heterochromatin from the nuclear periphery in *Caenorhabditis elegans* embryos. Analysis of histone methyltransferases (HMTs) showed that elimination of two HMTs, MET-2 and SET-25, mimics the loss of SAM synthetase, abrogating the perinuclear attachment of heterochromatic transgenes and of native chromosomal arms rich in histone H3 lysine 9 methylation. The two HMTs target H3K9 in a consecutive fashion: MET-2, a SETDB1 homolog, mediates mono- and dimethylation, and SET-25, a previously uncharacterized HMT, deposits H3K9me3. SET-25 colocalizes with its own product in perinuclear foci, in a manner dependent on H3K9me3, but not on its catalytic domain. This colocalization suggests an autonomous, self-reinforcing mechanism for the establishment and propagation of repeat-rich heterochromatin.

INTRODUCTION

Transcriptional control of the eukaryotic genome involves the differential organization of chromatin into euchromatic and heterochromatic domains (Kind and van Steensel, 2010). These two active and silent compartments differ in characteristic posttranslational modifications of the core histones, as well as in the incorporation of specific histone variants, linker histones, and nonhistone proteins. Trimethylation of lysine 9 on histone H3 (H3K9me3) or H3K27me3 is associated with silent domains, whereas euchromatin is enriched for acetylated histones and H3K4me3 (Black and Whetstine, 2011).

From yeast to man, euchromatin and heterochromatin are spatially segregated within the nucleus. In metazoans, repeat-containing centromeric heterochromatin is typically clustered into foci that are enriched for H3K9me3 and Heterochromatin protein 1 (HP1) (Maison and Almouzni, 2004). Similarly, the Polycomb repressor complex is found in nuclear foci that bear H3K27me3 (Luo et al., 2009). A distinct type of heterochromatin enriched for both H3K9 and H3K27 methylation binds the nuclear lamina (Kind and van Steensel, 2010), a meshwork of intermediate filament proteins and several lamin-associated factors that underpin the inner nuclear membrane (INM) (Goldman et al., 2002). Genome-wide analysis has shown that lamin-bound heterochromatin comprises up to 40% of the mammalian genome and occurs in lamin-associated domains (LADs) that often span several megabases in *cis* (Guelen et al., 2008; Peric-Hupkes et al., 2010). Similarly, in the nematode *Caenorhabditis elegans*, LADs cover large regions of the repeat-rich distal third of all chromosome arms (Ikegami et al., 2010).

Downregulation of *C. elegans* lamin, or of the lamin-associated proteins EMR-1 and LEM-2, leads to the derepression of promoters on perinuclear heterochromatic arrays (Mattout et al., 2011). In flies as well, lamin is required to repress testis-specific genes in somatic tissues (Shevelyov et al., 2009), suggesting that the attachment of a locus to the nuclear lamina can affect its expression. In support of this, artificial relocation of genes to the nuclear lamina contributes to their transcriptional repression in mammals and flies, although in a promoter-specific manner (reviewed in Kind and van Steensel, 2010). How this is achieved is unclear.

To understand the functional implications of chromatin attachment to the INM one must identify and interfere with the factors involved. Only a few lamin ligands with chromatin binding capacity have been described. One example, BAF (barrier to autointegration factor), binds both histones and DNA and associates with the lamin-interacting INM proteins LAP2, MAN1, and Emerin (Margalit et al., 2007). A second example is HP-1, which binds the INM-associated Lamin B receptor (Ye and Worman,

1996). The relevance of these interactions in vivo and how they might selectively recruit genes to the nuclear periphery remain unclear.

Repetitive gene arrays have been useful tools to study the mechanism and dynamics of perinuclear heterochromatin anchoring (Meister et al., 2010; Yuzyuk et al., 2009). In worms, as well as in mammals, transgene arrays are frequently subject to transcriptional repression (Hsieh and Fire, 2000; Martin and Whitelaw, 1996) and accumulate repressive histone marks, namely histone H3K9me3 and H3K27me3 (Bessler et al., 2010; Meister et al., 2010). Most important for this study, repetitive arrays integrated into the worm genome recapitulate the perinuclear sequestration of endogenous heterochromatin on chromosome arms.

Here, we used such gene arrays in a genome-wide RNAi screen to identify conserved factors required for the anchoring of heterochromatin. This screen yielded a single RNAi target whose loss impaired both repression and anchoring in *C. elegans* embryos. The target encodes S-adenosyl methionine synthetase, which generates S-adenosylmethionine (SAM), the universal donor for methylation reactions in eukaryotic cells. Given that interference with SAM synthesis caused a drop in histone methylation, we systematically monitored the roles of histone methyl transferases (HMTs) and found that the peripheral anchoring of arrays depends on two HMTs, MET-2 and SET-25, both of which target H3K9. Consistently, endogenous domains of H3K9 methylation on chromosome arms were released from the nuclear lamina in the *met-2 set-25* double mutant.

We show that MET-2, a SETDB1 homolog, deposits mono- and dimethyl groups at H3K9, whereas SET-25, a previously uncharacterized HMT, trimethylates the same residue. SET-25 colocalizes with peripheral heterochromatin in an H3K9me3-dependent fashion, thus becoming sequestered at the nuclear periphery by the product of its own methylation reaction. The increased concentration of SET-25 in perinuclear heterochromatin is compatible with a self-reinforcing mechanism, whereby this enzyme acts to establish and stabilize heterochromatic repression at the nuclear periphery.

RESULTS

A Genome-Wide RNAi Screen Identifies Regulators of Gene Array Silencing in *C. elegans* Embryos

To identify factors required for perinuclear sequestration of heterochromatin, we designed a genetic screen, in which we monitored the derepression and relocalization of two genomically integrated gene arrays in *C. elegans* embryos at the 50- to 100-cell stage. Both arrays encode green fluorescent protein (GFP) under the control of a ubiquitously expressed promoter (either the *let-858* or the *baf-1* promoter). Each reporter was integrated in approximately 300 copies at a single site in the genome, generating a transcriptionally repressed locus bearing the heterochromatic histone modifications H3K9me3 and H3K27me3 (Bessler et al., 2010; Meister et al., 2010).

In a strain that is homozygous for an integrated *let-858::GFP* gene array, we downregulated 80% of all *C. elegans* genes by RNAi and selected clones that could derepress the ubiquitously active *let-858::GFP* reporter in embryos (Figure 1A). Specifically, synchronized L1 worms carrying the array were exposed to RNAi for 4 days (Kamath et al., 2003). As the larvae developed to gravid adults, we visually inspected the embryonic progeny in utero for increased GFP expression (Figure 1A). We retained only hits that caused array upregulation throughout embryonic cell types. Similarly, we discarded clones targeting essential genes (based on Kamath et al., 2003) because embryonic lethality often led to an unspecific deregulation of the *let-858::GFP* transgene in a small number of cells per embryo (unpublished observation). Viable hits were retested in triplicate next to negative controls on the same plate. We identified 29 RNAi clones that reproducibly caused array derepression in at least two out of three replicates without inducing embryonic death (Table S1; Figure 1C). These 29 hits were enriched for chromatin factors (Figure 1C; $p = 9.7 \times 10^{-4}$, DAVID gene ontology term enrichment, Dennis et al., 2003), including two histone methyl transferases (*mes-4* and *set-25*), three histone binding proteins (*mrg-1*, *lin-61*, *hpl-2*), and the Polycomb repressor complex 2 (PRC2) components *mes-3* and *mes-6*. The catalytic subunit of PRC2, *mes-2*, was among the 20% of genes that were not covered by the RNAi library used for this screen, but an analysis of mutant alleles confirmed derepression upon loss of *mes-2* as well (see below; Figure S2B available online).

Depletion of Two Related S-Adenosylmethionine Synthetases Causes Array Detachment

We subsequently used confocal microscopy to test which of the factors involved in array repression were also required to position arrays at the nuclear periphery (Figure 1B). To this end, we used a second array (termed *gwIs4*), which contains 300 copies of the ubiquitously active *baf-1* promoter driving the expression of GFP fused to the bacterial repressor LacI (Meister et al., 2010). Each plasmid copy within the *gwIs4* array contained a *lacO* site, allowing the GFP-LacI protein to bind the transgene array from which it is expressed, generating a focus visible by fluorescence microscopy (Meister et al., 2010; Figure 1B). This array thus serves a dual purpose: total GFP levels monitor the expression level of the *baf-1* promoter, whereas the position of the GFP-LacI focus marks the position of the array relative to the nuclear periphery.

Visual inspection by confocal microscopy revealed that arrays were displaced from the nuclear periphery in only two of the 29 primary hits. Both positive clones targeted the SAM synthetases *sams-3* and *sams-4* (Figures 2A–2D). Because the two genes share extensive homology with each other (100% identity over 665 nucleotides of coding sequence, Figure S1A), including the sequences targeted by the RNAi, it was clear that each RNAi clone alone downregulated both genes. Therefore, for all subsequent experiments a single RNAi clone (*sams-3)* was used.

To quantify the degree of array detachment upon *sams-3/4* downregulation, we acquired focal stacks of RNAi-treated embryos. We determined the radial distribution of GFP-foci by binning the spots into three concentric zones of equal surface area in the focal plane with the highest GFP-spot intensity (Figure 2E). For spherical nuclei, this method yields an equal distribution among the three zones for a randomly positioned focus (Meister et al., 2010). Whereas the *gwIs4* array was strongly

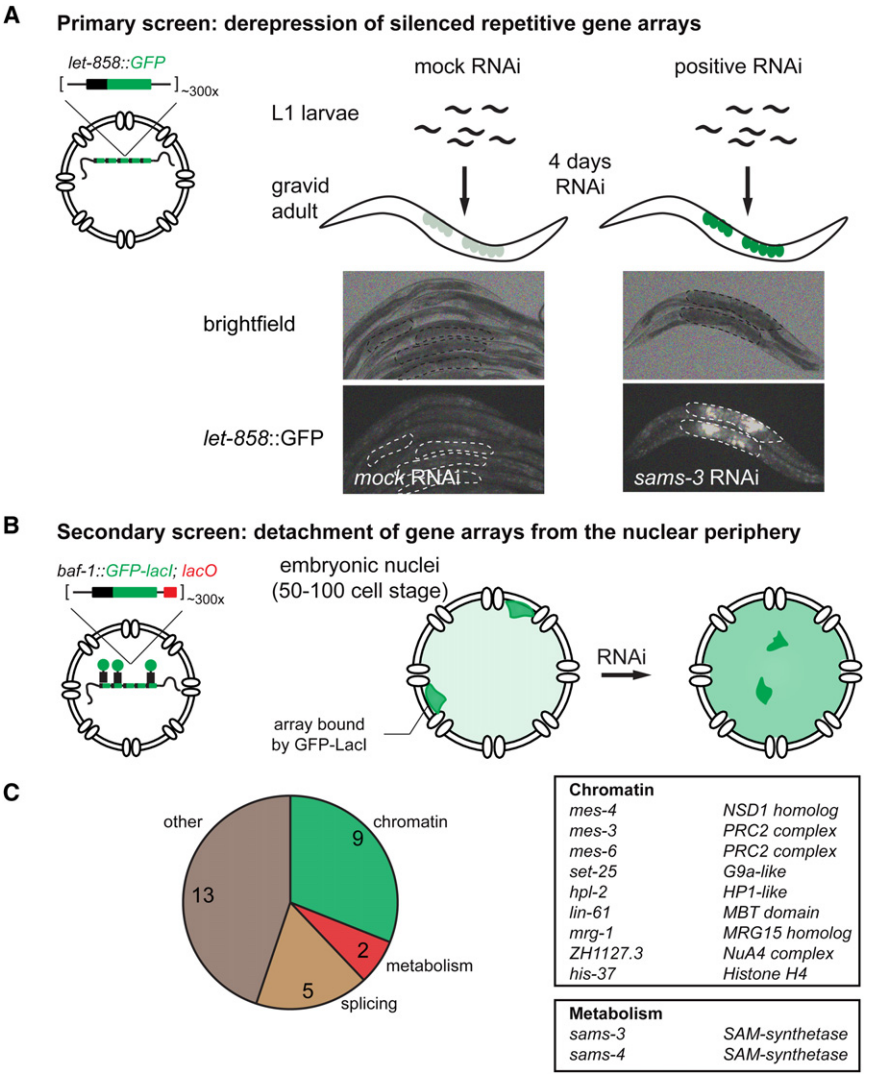

Figure 1. Design of a High-Throughput Two-Step RNAi Screen to Identify Factors Involved in Perinuclear Chromatin Anchoring

(A) Primary screen for derepression of array-borne promoters. L1 larvae of strain NL2507 carrying the repetitive transgene *pkIs1582[let-858::GFP; rol-6(su1006)]* were subjected to all clones of a genome-wide RNAi library. After 4 days, the embryonic progeny within their uterus was screened for increased levels of GFP, exemplified by *sams-3* RNAi.

(B) Secondary screen for gene array detachment. Strain GW566 carrying the *gwIs4[baf-1::GFP-lacI;myo-3::RFP]* transgene was subjected for 4 days to RNAi against all hits of the primary screen described in (A). The *gwIs4* transgene contains *lacO* sites, which are bound by GFP-LacI, such that the transgene position can be determined microscopically.

(C) Summary and classification of the hits of the primary screen. Selected hits are shown, and the complete list is in Table S1.

enriched in the most peripheral zone in embryos treated with control RNAi (>90% in zone 1; Figure 2F, left, gray bars), the array consistently shifted toward the nuclear center after *sams-3/4* RNAi (<25% in zone 1, $p < 2.45 \times 10^{-11}$, Fisher's exact test; Figure 2F, left, black bars).

To see whether array detachment upon *sams-3/4* RNAi required activation of an array-borne promoter, we repeated the *sams-3/4* RNAi experiment with an array that carried two tissue-specific promoters, namely a truncated *pha-4* promoter driving LacZ and the *rol-6* gene, instead of the *baf-1* promoter. Both of these tissue-specific promoters are silent in most early embryonic cells (Azzaria et al., 1996; Sassi et al., 2005). To visualize the array, we expressed GFP-LacI in *trans* from an independent transgene that lacked *lacO* sites. As observed for the *gwIs4* array, depletion of SAMS-3/4 abrogated the association of the [*pha-4::lacZ;rol-6*] array with the INM (Figure 2F, right), yet *pha-4::lacZ* remained silent in all cells except the four to eight intestinal precursor cells that expressed the factors necessary for *pha-4* promoter induction (Figure S1B). Because the array was efficiently delocalized in all cells, we conclude that array detachment from the INM arising from the downregulation of SAMS-3/4 synthetases can occur independently of transcriptional activation.

We did not observe array detachment for any of the other 27 primary screen hits that showed derepression of the array-borne GFP reporter. This argues against the simple explanation that transcriptional activation drives array delocalization. To ensure that the persistence of derepressed arrays at the INM was not due to inefficient RNAi, we generated strains carrying the *gwIs4* array and a genetic null allele of a subset of the screen hits. Using genetic null mutants, we observed a 20% drop in array attachment in the *set-25* mutant (70% bound, Figure 3B; see below). For all other mutants, including the H3K27 and H3K36 HMTs *mes-2* and *mes-4*, arrays remained firmly anchored at the nuclear periphery (Figures 3B and S2B and S2C). We conclude that transgene array derepression is neither sufficient nor necessary for detachment. This does not exclude, of course, roles for other factors that are either redundant or insufficiently sensitive to RNAi, in array anchoring.

High Levels of SAM Synthetase Are Required for Normal Histone Methylation

The enzymes SAMS-3/4 generate SAM, the unique cellular methyl-group donor. Although there are other, more divergent SAM synthetases in the *C. elegans* genome, the downregulation of *sams-3/4* is expected to reduce cellular methylation, including that on histones. Because specific histone H3 methylation sites are robustly associated with heterochromatic

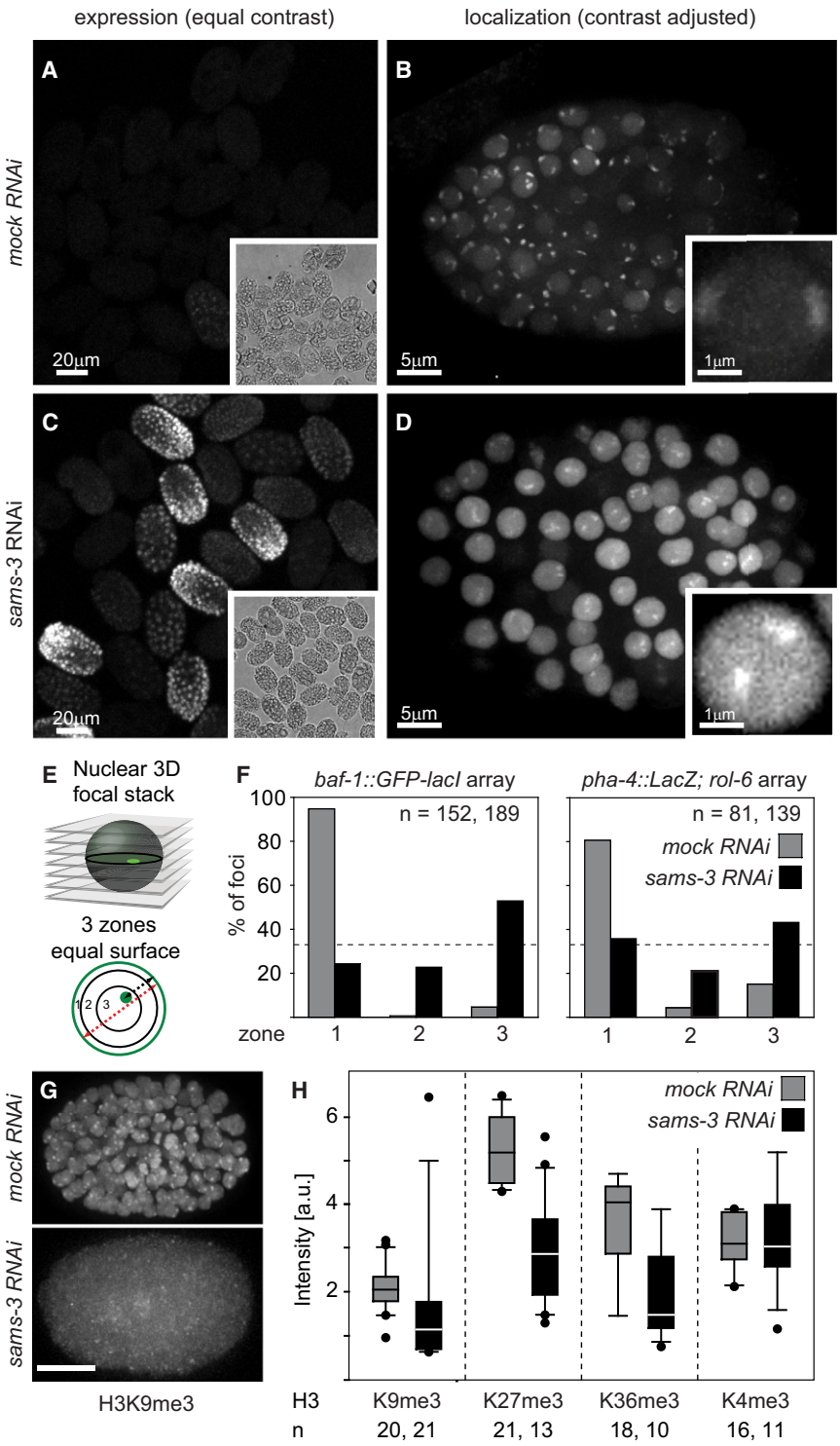

Figure 2. Depletion of SAM Synthetases Globally Reduces Histone Methylation Coincident with Array Derepression and Detachment

(A and C) The *gwIs4[baf-1::GFP-LacI]* transgene is strongly derepressed upon *sams-3* RNAi. Shown are the GFP and brightfield (inset) signal of many embryos. Control and *sams-3* RNAi were imaged at the same illumination settings and are displayed with the same contrast.

(B and D) z-projection of representative embryos carrying the *gwIs4* array after *sams-3* and control RNAi. Significant array detachment is observed for *sams-3* but not for control RNAi. Insets show a single focal plane of one nucleus.

(E) Array distribution is scored in a three-zone assay using the focal plane in which the spot has the highest intensity. Each cross-section was divided into three concentric zones of equal surface. Foci from many nuclei were binned into the three zones. A random distribution gives 33% per zone.

(F) Quantification of array distribution as in (E). Significant array detachment upon *sams-3* RNAi is observed for the *baf-1::GFP-lacI* array (left) and for the *pha-4:LacZ; rol-6* array (right), which lacks active housekeeping promoters ($p < 2.45 \times 10^{-11}$, Fisher's exact test). n, foci scored per condition; dotted line, expected random distribution.

(G) Embryos treated with *sams-3* and control RNAi stained for H3K9me3. Scale bar, 5 µm

(H) Quantification of fluorescence intensities from the indicated number of embryos (n), stained for the indicated histone methyl marks. H3K9, H3K27, and H3K36 me3 is significantly reduced upon RNAi ($p \leq 0.004$, rank sum test). H3K4me3 did not change significantly ($p = 0.846$). Whiskers: 10th and 90th percentile; black dots: outliers; horizontal line: median.

See also Figure S1.

arrays (Bessler et al., 2010; Meister et al., 2010), we probed RNAi-treated embryos with antibodies specific for a range of methylated histones, namely trimethylated K4, K9, K27, and K36 on histone H3. The fluorescent immunostaining of methylated histone H3K9, K27, and K36 was strongly reduced, often to a point below the background signal (Figures 2G, 2H, and S1C). Interestingly, we did not detect a strong reduction in trimethylation of H3K4 (Figures 2H and S1C), although we cannot exclude that the high residual signal after *sams-3/4* RNAi stems from off-target antibody binding. Alternatively, the H3K4 methyltransferase may be less sensitive to reduced SAM levels than are other HMTs.

Remarkably, the severe reduction in methylation of H3K9, K27, and K36 provoked by *sams-3/4* RNAi was compatible with embryonic development. We did not observe an increase in embryonic lethality after *sams-3/4* depletion for up to three generations, although we did detect a significant reduction in brood size (Figure S1D). This is consistent with results showing that HMT mutations affecting H3K9, K27, and K36 methylation have relatively mild somatic defects but much stronger phenotypes in

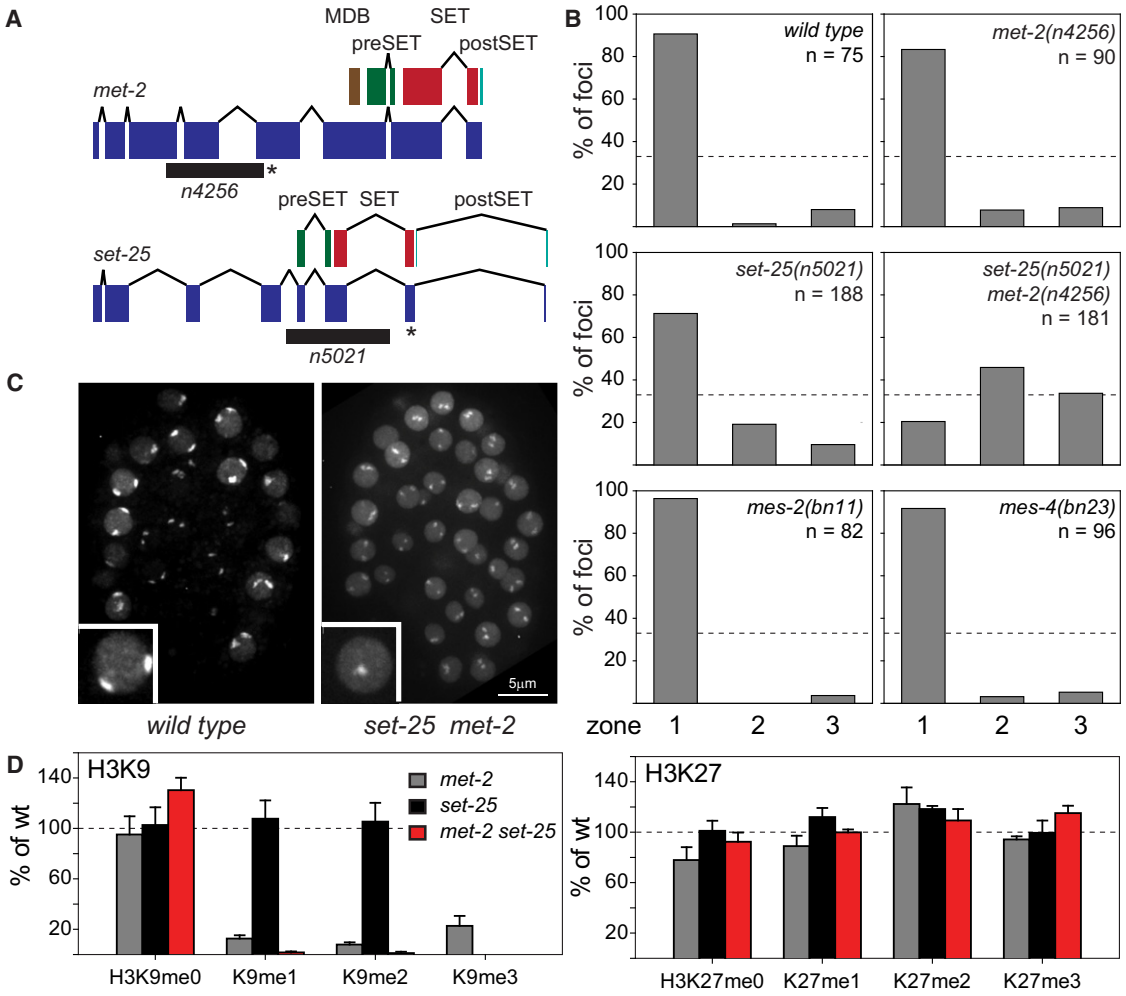

Figure 3. H3K9 Methyltransferases MET-2 and SET-25 Are Required for Gene Array Anchoring

(A) Scheme of *met-2* and *set-25* exon and domain structure, and deletion alleles used. * STOP codon caused by frame shift.

(B) Quantification of array distribution in 50–100 cell embryos as described in Figure 2E. Significant array detachment occurs in *set-25* and *set-25 met-2* but not in *mes-2* and *mes-4* mutants ($p \leq 8 \times 10^{-4}$ for comparisons: *set-25* versus wild-type, *set-25 met-2* versus wild-type, and *set-25* versus *set-25 met-2*; $p \geq 0.16$ for comparisons wild-type versus *met-2*, wild-type versus *mes-2*, and wild-type versus *mes-4*, Fisher's exact test). Dotted line, expected random distribution.

(C) Partial z-projection of GFP signal of wild-type and *set-25(n5021) met-2(n4256)* double-mutant embryos carrying the *gwIs4[baf-1::GFP-LacI]* array.

(D) Quantification of H3K9 and H3K27 methylation levels in *met-2* and *set-25* single- and double-mutant early embryos by quantitative mass spectrometry. Data are shown relative to wild-type (dotted line, 100%). Error bars indicate the SEM in positive direction from three biological replica. See also Figures S2 and S3 and Tables S2 and S4.

the germline (Andersen and Horvitz, 2007; Bender et al., 2004; Bender et al., 2006).

In addition to *sams-3* and *sams-4*, the *C. elegans* genome encodes two more divergent SAM synthetases (*sams-1* and *sams-5*). RNAi of *sams-3/4* in a *sams-1/5* double mutant was not compatible with somatic growth, causing larval arrest at high penetrance (Figure S1E). Hence, despite the presence of multiple, partially redundant enzymes in *C. elegans*, downregulation of the enzymes SAMS-3 and SAMS-4 reduced SAM sufficiently to have a pronounced effect on histone methylation and transgene array localization while supporting embryonic development.

The Methyltransferases MET-2 and SET-25 Act Redundantly to Position Chromatin at the Nuclear Periphery

To test whether histone methylation itself is required for perinuclear chromatin anchoring, we next focused specifically on HMT mutants. We retrieved loss-of-function alleles for all HMTs identified in our primary screen, as well as for those predicted to target the same histone residues. Using this genetic resource, we scored for defects in heterochromatic array attachment at the INM in 11 different strains carrying mutations for individual or multiple SET domain proteins (Table S2). The tested single and double mutants included all known HMTs that target

H3K9, K27, K36, or combinations of multiple of these, all of which yielded viable embryos. For mutations in *mes-2* and *mes-4*, which cause maternal effect sterility (Capowski et al., 1991), we scored embryos of the second homozygous generation, which lack both maternal and zygotic MES proteins.

Ten out of the 11 single and double mutants tested were defective in array silencing, albeit not all to the same degree (Figure S2B; Table S2). However, arrays remained peripheral in all but two strains (Figure 3B; Table S2). The only single mutant with even partial array detachment was a *set-25* deletion (Figure 3B). Although the effect of *set-25* mutation on array position was significant ($p < 8 \times 10^{-4}$), 70% of the arrays nonetheless remained at the nuclear periphery in this mutant (Figure 3B). Complete release of arrays was only seen when we additionally deleted *met-2*, another HMT. Notably, the mutation of *met-2* alone did not cause significant array detachment and only mildly derepressed it (Figures 3B and S2A and S2B).

We confirmed that the observed array detachment in the double *set-25 met-2* mutant did not stem from allele-specific effects, or an unrelated background mutation, by scoring transgene position in another deletion allele of *met-2* combined with a *set-25* mutation and in a *met-2* mutant treated with *set-25* RNAi (Figure S2E). All three deletion alleles either span the SET domain or introduce a premature stop codon upstream of it (Figure S2D). These results allow us to conclude that *met-2* and *set-25* function redundantly to promote perinuclear localization and gene array silencing in *C. elegans* embryos. Loss of both recapitulates the loss of heterochromatin anchoring phenotype associated with *sams-3/-4* RNAi.

met-2 and *set-25* Are Required for Mono-, Di- and Trimethylation of H3K9

The SET domain of SET-25 is homologous to the mammalian enzymes EHMT1/G9a (28.8% identity, 44.6% similarity) and Suv39h1/2 (27.9% identity, 45.7% similarity), which both target histone H3K9 (Rea et al., 2000; Tachibana et al., 2002). SET-25, however, lacks both the Chromodomain and the Ankyrin repeats present in Suv39h1/2 or G9a (Figure 3A). Similarly, MET-2 is homologous to the mammalian H3K9 HMT SETDB1 (Andersen and Horvitz, 2007; Bessler et al., 2010). This suggests that MET-2 and SET-25 target H3K9, although additional nonhistone targets may exist.

To test whether the deletion of *met-2* and *set-25* indeed altered specific histone methylation states, we measured global histone methylation in early *C. elegans* embryos carrying mutations in either *met-2*, *set-25*, or in both genes by relative quantification using LC-MRM mass spectrometry. We found no systematic differences in the methylation levels of H3K23, K27, or K36 in either single or double mutants, but we found striking changes in the methylation of H3K9 (Figures 3D and S3). In agreement with previous reports (Andersen and Horvitz, 2007; Bessler et al., 2010), mono-, di-, and trimethylation of H3K9 were all reduced in the *met-2* single mutant, although each could be detected at 10% to 30% of wild-type levels (Figure 3D). In the *set-25* single mutant, on the other hand, H3K9me1 and me2 were at wild-type levels, whereas no H3K9me3 could be scored. Importantly, in the *met-2 set-25* double mutant, we could detect no mono-, di- or trimethylation of H3K9 whatsoever (Figure 3D). This shows that there are no other histone H3K9 methyltransferase activities in the worm embryo and allows us to conclude that in the absence of SET-25, MET-2 catalyzes only H3K9 mono- and dimethylation. Moreover, whereas SET-25 alone can generate all three methylation states, its efficiency for H3K9 trimethylation is strongly increased when H3K9me1/2 is provided by MET-2. Together these data suggest that the two enzymes act in a step-wise manner. First, MET-2 mono- and dimethylates H3K9. Subsequently, SET-25 uses H3K9me1/2 as a substrate for trimethylation.

Heterochromatin anchoring was only partially compromised in the absence of SET-25 but was completely lost in the double mutant (Figure 3B). This suggests that H3K9me1/2 is sufficient to anchor ~70% of the arrays at the INM in the *C. elegans* embryo (versus 90% in wild-type). Even though the arrays remained peripheral in the absence of H3K9me3 arrays, they were strongly derepressed (Figure 3B and S2A and S2B). Trimethylation of H3K9 on peripheral arrays by SET-25 is therefore crucial for efficient array repression but anchoring can be mediated by either H3K9me1/2 or H3K9me3.

Mass spectrometry of histones from L1 larvae also showed strongly reduced levels of H3K9 methylation in the *set-25 met-2* double mutant, yet peripheral anchoring in these differentiated cells was affected to a much smaller degree (Figures S2F and S3). This suggests that additional anchoring mechanisms exist in differentiated tissues that may not rely exclusively on H3K9 methylation.

H3K9me1 and me2 Are Enriched at the Nuclear Periphery, Independently of H3K9me3

We next asked whether endogenous genomic domains carrying H3K9 methylation are similarly enriched at the INM. To test this, we localized H3K9me1, me2, and me3, and total histone H3 by indirect immunofluorescence with specific antibodies (Figure S4A) in the nuclei of wild-type and *set-25* mutant embryos lacking a transgene array. We counterstained the INM with antibodies for either *C. elegans* lamin (LMN-1) or nuclear pores (Figure 4A).

We measured ~150 H3K9 methylation profiles across the nuclear diameter of the equatorial focal plane of embryonic nuclei. As expected, the distribution of total histone H3 was identical to that of the DNA signal. In contrast, all three methylated forms of H3K9 showed enrichment at the nuclear periphery (Figure 4B, left). Repeating the same analysis in the *set-25* mutant, in which we detected no H3K9me3, revealed persistent perinuclear enrichment of H3K9me1 and H3K9me2 (Figure 4B, right). This is consistent with the INM attachment observed for gene arrays in the absence of H3K9me3 and suggests that endogenous domains carrying H3K9me1/2 bind the nuclear envelope independently of H3K9me3.

Mutation of *met-2* and *set-25* Globally Reduces Lamin Interaction of Chromosome Arms

We next asked whether the positioning of endogenous domains bearing H3K9 methylation is similarly sensitive to the loss of SET-25 and MET-2. In the worm, H3K9 methylation is enriched in the distal third of each chromosome arm (Liu et al., 2011; Figure 5C). In agreement with our proposal that H3K9me

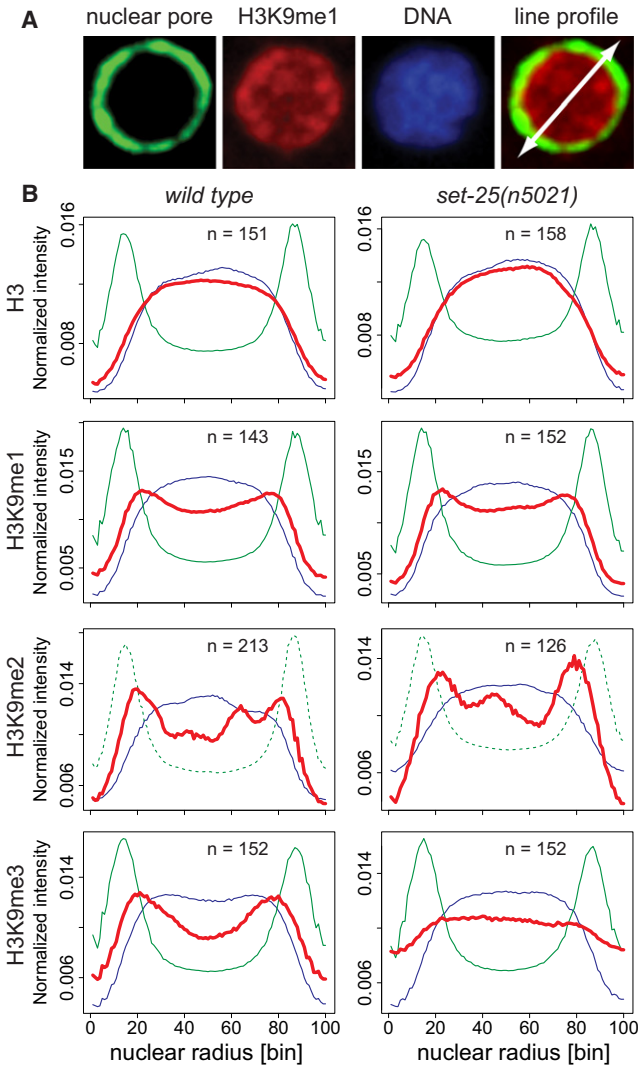

Figure 4. H3K9me1, me2, and me3 Are Enriched at the INM Independent of *set-25*

(A) Representative nuclear central focal plane of a wild-type embryo stained for H3K9me1 and the nuclear pore.

(B) Quantification of radial intensity of staining in wild-type and *set-25(n5021)* mutant embryos as described in Experimental Procedures. Embryos were stained for the indicated histone modification (red), DNA (blue), and LMN-1 (green dotted) or the nuclear pore (green). For each panel, the indicated number (n) of radial line profiles was scaled and pooled into 100 bins, normalized, and averaged. The nearly flat curve for H3K9me3 in the right panel reflects the absence of this mark in the *set-25* mutant.

See also Figure S4.

serves as a trigger for perinuclear chromatin anchoring, H3K9me-rich chromosome arms were found to coimmunoprecipitate with LEM-2, a lamin-associated component of the INM (Ikegami et al., 2010). To see whether H3K9me contributes to the peripheral localization of these endogenous domains, we applied lamin-DamID (Pickersgill et al., 2006) to probe their subnuclear position in wild-type and *set-25 met-2* mutant worm embryos.

Specifically, we expressed a fusion protein between *C. elegans* lamin (LMN-1) and the *E. coli* adenine DNA methyltransferase (Dam) at low levels in *C. elegans* embryos. The LMN-1-Dam fusion was incorporated into the endogenous lamin meshwork at the nuclear periphery (data not shown) where it preferentially methylated DNA in close proximity. We amplified adenine methylated DNA by PCR from three biological replicas of each genotype and hybridized it to genomic tiling arrays by using DNA extracted from strains expressing a freely diffusible Dam-GFP fusion as competitor. This neutralizes the impact of sequence context on Dam activity.

Consistent with published chromatin immunoprecipitation (ChIP) results for the lamin interacting factor LEM-2 (Ikegami et al., 2010), we found that the LMN-1-DamID signal was strongly enriched on the arms of all autosomes and on the left arm of the X chromosome in wild-type embryos (Figure 5A, black line). In contrast, the enrichment of the LMN-1-DamID signal on chromosome arms as compared to central domains was significantly reduced in the *set-25 met-2* double mutant (Figure 5A, red line). This argues that the methylation deposited by SET-25 and MET-2 plays a role in the peripheral positioning of endogenous heterochromatin.

Intriguingly, the magnitude of reduction in LMN-1 DamID upon mutation of *met-2* and *set-25* was correlated with levels of H3K9 methylation in wild-type cells (Figure 5D and S5A). The more enriched for H3K9 methylation, the stronger the effect of the double mutant. This suggests that regions on chromosome arms with low H3K9me (e.g., ChrIV-R) use an alternative anchoring mechanism that is independent of this mark that accounts for the residual enrichment of LMN-1 on the distal chromosome arms in the *set-25 met-2* double mutant. Interestingly, positioning of the X chromosome was completely insensitive to loss of H3K9 methylation (Figure 5A).

To verify that domains with either high or low H3K9 methylation levels behave differentially in response to the double mutant, we measured the subnuclear position of two loci on the right arm of chromosome V (ChrV-R) by fluorescence in situ hybridization (FISH) and microscopy. We first scored a 30 kb domain next to the C18D4.6 locus that lies in a region of very high H3K9me3 and showed strongly reduced LMN-1 interaction in the *set-25 met-2* mutant (Figures 5A and 5C). Indeed, 3D FISH confirmed that this locus shifted from a peripherally enriched to a near random distribution upon loss of H3K9 methylation (Figures 5E and 5F). On the other hand, for the *pha-4* locus, which is 170 kb away from the telomere of ChrV-R and has comparatively low levels of H3K9 methylation, we did not score a significant shift away from the nuclear lamina in the double mutant, either by DamID or by microscopy (Figures S5B and S5C). This suggests that the *pha-4* locus may be positioned at the INM by an H3K9me-independent mechanism.

Taken together, by lamin-DamID and by microscopy we confirm an important role of SET-25 and MET-2 HMTs and the mono-, di- and trimethylation of histone H3K9 in the anchoring of native chromosome arms. At the same time, we identify a residual anchoring pathway that confers H3K9-independent positioning.

We next compared gene expression of wild-type and *set-25 met-2* mutant embryos by using genome-wide expression

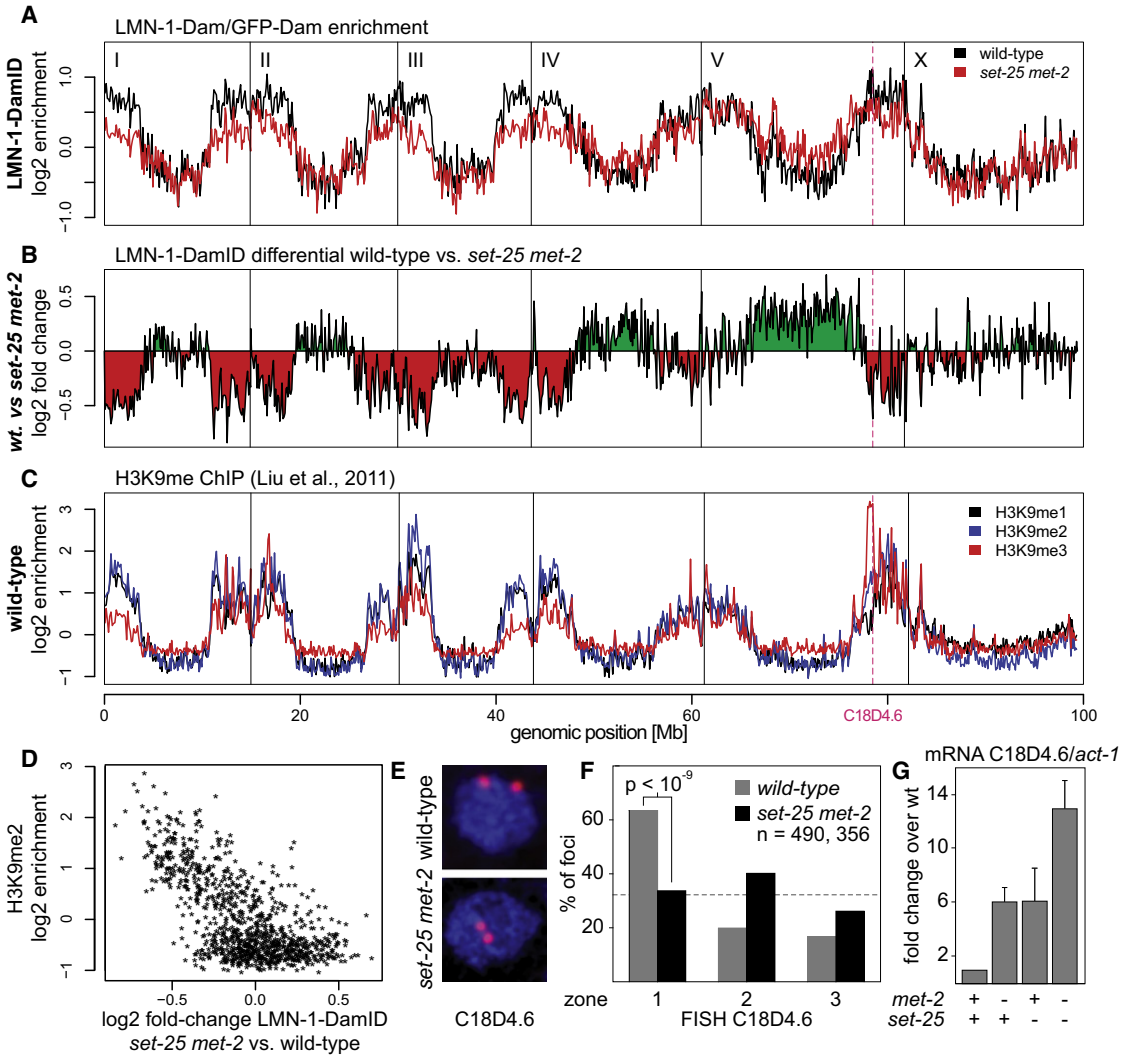

Figure 5. SET-25 and MET-2 Contribute to the Positioning of Chromosome Arms at the Nuclear Lamina

(A) LMN-1-Dam signal in wild-type (black) and *set-25 met-2* (red) embryos (averaged from three biological replica). Tracks for all six chromosomes are shown. The pink dashed line indicates the position of the FISH probe used in (E and F). Each point reflects mean signal averaged from 2,000 array probes spanning 150 kb.

(B) Differential of LMN-1-Dam signal from wild-type and *set-25 met-2* embryos.

(C) H3K9me1, me2, and me3 enrichment in early embryos (data from Liu et al., 2011).

(D) Changes in LMN-1-Dam methylation between wild-type and *set-25 met-2* mutant correlate with high levels of H3K9 methylation.

(E) Single focal plane of *set-25 met-2* and wild-type nuclei probed by FISH for the C18D4.6 locus (red) and counterstained for DNA (blue).

(F) Quantification of FISH signal shown in (E) by three-zone scoring. n, number of scored foci.

(G) Quantification of expression levels of the C18D4.6 gene in indicated mutants by quantitative PCR. Data are shown normalized to *act-1* and relative to expression in wild-type. Error bars indicate the SEM from three biological replicas.

See also Figure S5.

arrays. Consistent with our conclusion that transcriptional activity and position are not obligately linked, we did not find a strong genome-wide correlation of gene detachment and upregulation (data not shown). Nevertheless, among the genes upregulated in the double mutant, the C18D4.6 locus had strongly increased expression (12-fold) in the *set-25 met-2* mutant (Figure 5G). This indicates that subnuclear position mediated by H3K9me correlates with the silencing of some, but not all, genes.

MET-2 Is Enriched in the Cytoplasm

To examine the direct function of SET-25 and MET-2 in chromatin anchoring and silencing, we next studied the subcellular localization of the enzymes themselves. This was performed by expressing each enzyme as a fusion to mCherry (mCh). Both fusions were functional, as their expression in the *set-25* and *met-2* mutants restored H3K9 methylation (Figure S4B). Intriguingly, mCh-MET-2 was primarily cytoplasmic, whereas mCh-SET-25 was strongly enriched in the nucleus (Figure 6A).

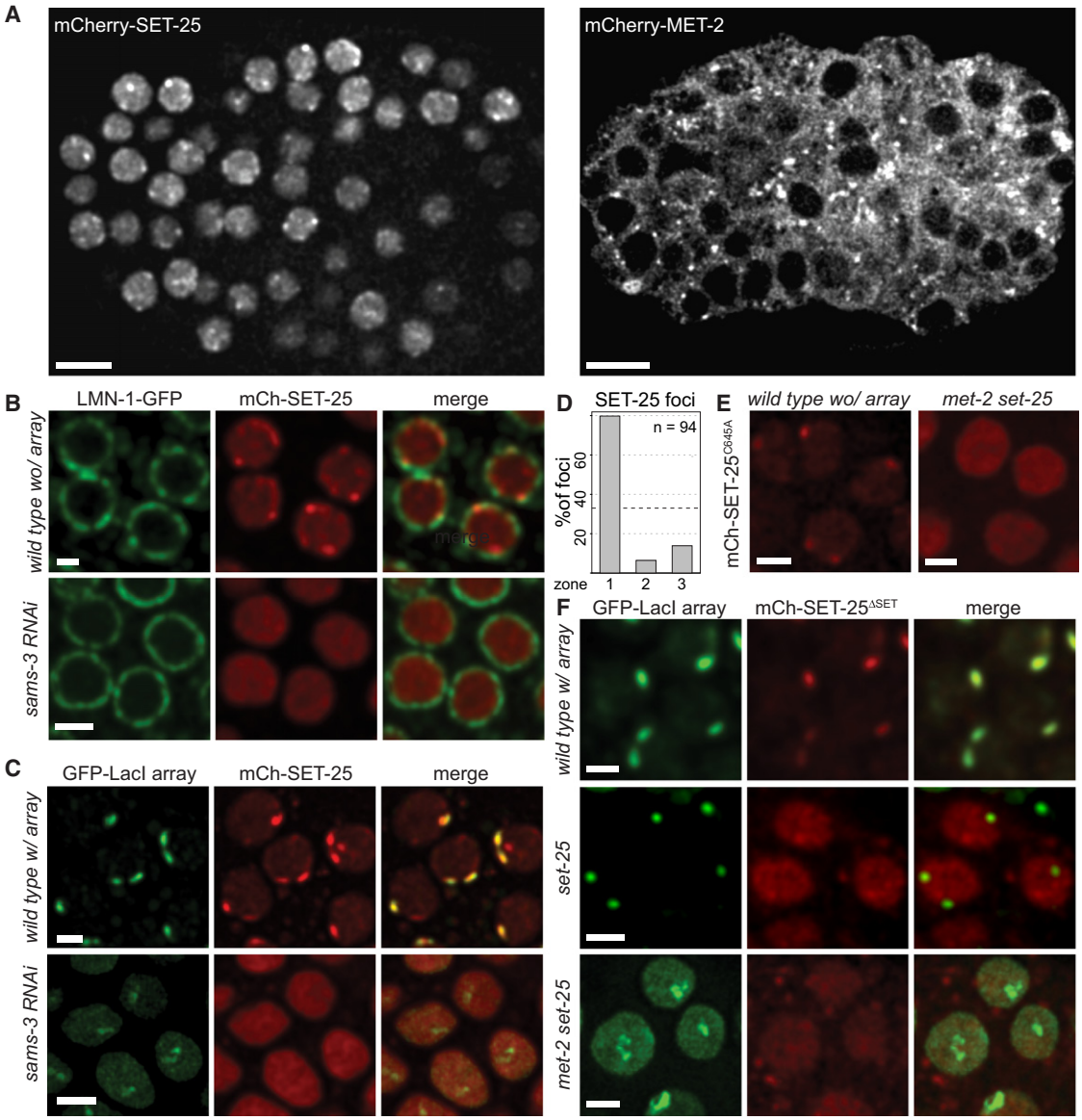

Figure 6. SET-25 Localizes to Perinuclear Foci in an H3K9 Methylation-Dependent Manner

(A) SET-25 and MET-2 were tagged N terminally with mCherry (mCh) and expressed in *C. elegans* embryos under control of the ubiquitously active *his-72* promoter. Scale bar, 5 μm.

(B and C) Representative nuclei of embryos expressing mCh-SET-25 as described in (A) under control and *sams-3* RNAi conditions. mCh-SET-25 forms perinuclear foci in the absence (B) and presence (C) of the *gwIs4* array. Strong SET-25 foci in C colocalize with the GFP-LacI signal that marks the *gwIs4* transgene. Peripheral SET-25 foci and array-associated SET-25 are dispersed upon *sams-3* RNAi.

(D) Quantification of the radial distribution of mCh-SET-25 foci as shown in B (top) by three-zone scoring (Figure 2E). SET-25 foci are significantly enriched at the nuclear envelope over a random distribution (dotted line, $p < 10^{-15}$, Fisher's exact test).

(E) Localization of mCh-SET-25-C645A mutant in wild-type and *met-2(n4256) set-25(n5021)* embryos.

(F) As in (C, bottom), but for mCh-SET-25$^{\Delta SET}$ and in wild-type, *set-25(n5021)* and *met-2(n4256) set-25(n5021)* embryo. (B, C, E and F). Scale bar, 2 μm.

See also Figure S6.

We scored an identical localization for MET-2 with either a C-terminal or an N-terminal tag (Figure S4C). It is therefore unlikely that the cytoplasmic localization of mCh-MET-2 is due to a disruption of normal protein function by mCherry. In the cytoplasm, MET-2 would methylate nonnucleosomal histones, similar to the role proposed for the cytoplasmic fraction of the mammalian MET-2 homolog SETDB1 (Loyola et al., 2006; Loyola et al., 2009). The cytoplasmic localization of MET-2 also agrees with the step-wise deposition of H3K9 methylation, as suggested by our mass spectrometry data (Figure 3D).

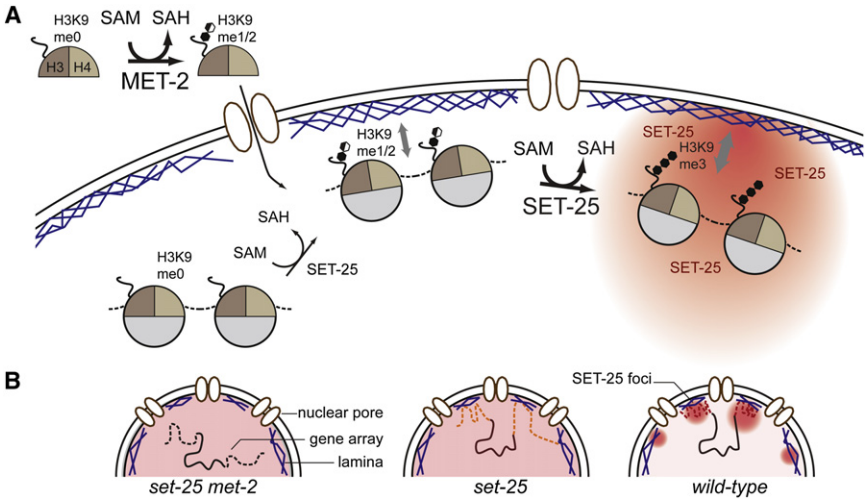

Figure 7. A Self-Reinforcing Mechanism for Perinuclear Anchoring and Heterochromatin Silencing

(A) The step-wise establishment of H3K9me3 involves deposition of H3K9me1/2 by cytoplasmic MET-2 prior to nucleosome assembly, and trimethylation by nuclear foci-associated SET-25. H3K9me1/2 initiates perinuclear chromatin targeting, and H3K9me3 is needed for complete array silencing and enhanced attachment. SET-25 requires its own reaction product, H3K9me3, to accumulate in perinuclear foci.

(B) The implications of (A) for the positioning of chromosome arms (dashed line) and generation of heterochromatic foci are shown. See Discussion for details.

SET-25 Localizes to Heterochromatic Perinuclear Foci

Careful inspection of mCh-SET-25 localization revealed that it was enriched in subnuclear foci that were often located at the nuclear periphery (80% in zone 1, Figures 6B and 6D) and which colocalized with both H3K9me3 and the worm HP1 homolog HPL-1 (Figure S6A). We did not see overlap of mCh-SET-25 and HPL-2 foci (Figure S6A), confirming that HPL-1 and HPL-2 occupy distinct subnuclear domains and have nonredundant functions (Schott et al., 2006).

Although mRNA levels of transgenic mCh-SET-25 were significantly higher than endogenous SET-25 (data not shown), the appearance of mCh-SET-25 foci is not simply a result of its expression level. Notably, we find that SET-25 foci are completely dispersed in embryos depleted for *sams-3* but have equal or even higher levels of mCh-SET-25 expression (see below). More importantly, the overexpressed mCh-SET-25 protein is functional because it rescued the loss of H3K9me3 in the *met-2 set-25* mutant (Figure S4B). To see whether the SET-25 foci correspond to heterochromatic domains, we next expressed mCh-SET-25 in embryos carrying the repetitive *gwIs4* array. In this strain, over the weaker perinuclear signal stemming from endogenous SET-25 foci, mCh-SET-25 formed two very bright foci that precisely colocalized with the GFP-LacI signal in every cell (Figure 6C).

SET-25 Localization Depends on H3K9 Methylation, but Is Independent of Its SET Domain

The colocalization of SET-25 with H3K9me3 and its enrichment on repetitive transgene arrays prompted us to test whether SET-25 localization was dependent on H3K9 methylation. Indeed, upon depletion of *sams-3/4* mCh-SET-25 distribution became diffuse, and it no longer accumulated in subnuclear foci (Figures 6B and 6C). To test whether SET-25 foci depend specifically on H3K9 methylation, we created a point mutation in the catalytic site of SET-25 (C645A), which corresponds to a catalytic null mutation in the homologous SET domain of human Suv39h (Rea et al., 2000). Like the wild-type mCh-SET-25, the C645A mutant still formed perinuclear foci, yet mCh-SET-25-C645A was completely dispersed in the *met-2 set-25* mutant, which specifically loses H3K9 methylation (Figure 6E). We conclude that SET-25 enrichment at the INM and focus formation are dependent on methylated H3K9 yet do not require that the bound SET-25 itself is catalytically active.

Given that SET-25 has no obvious methyl-binding domain, we tested whether its recruitment to peripheral foci would depend on its SET domain. To this end, we expressed an mCh-SET-25 fusion that was truncated upstream of the SET domain (SET-25$^{\Delta SET}$) in a strain carrying the repetitive gene array *gwIs4*. Like full-length SET-25, SET-25$^{\Delta SET}$ was strongly enriched on the *gwIs4* array (Figure 6F) and was dispersed in both a *met-2 set-25* double mutant and the *set-25* single mutant that lose H3K9me3 (Figure 6F and S6C). We conclude that the localization of SET-25 to perinuclear foci involves molecular interactions outside its catalytic domain and requires H3K9me3.

We can exclude that SET-25 is recruited to H3K9me3 by the Chromodomain-containing HP1 homologs HPL-1 and HPL-2. Although SET-25 colocalizes with HPL-1, it remained enriched on the *gwIs4* array in endogenous perinuclear foci in the *hpl-1 hpl-2* double-deletion strain (Figure S6B). Because we have not seen a specific direct interaction of SET-25$^{\Delta SET}$ with H3K9me3 in peptide binding assays (data not shown), we propose that SET-25 acts in a complex with other factors.

In summary, our results show H3K9me-dependent recruitment of gene arrays and chromosome arms to the nuclear envelope. SET-25, which deposits trimethylation, becomes enriched in H3K9me3 foci at the nuclear periphery, in a manner dependent on its own reaction product. This circularity could generate a self-sustaining subnuclear compartment that is enriched for H3K9 HMT activity, which in turn stabilizes silencing by efficiently trimethylating H3K9me1 and me2 (Figure 7).

DISCUSSION

Methylation of H3K9 Provides a Molecular Signal for Perinuclear Chromatin Localization

The eukaryotic nucleus shows remarkable spatial organization, with heterochromatin often associated with the nuclear envelope (NE) (Akhtar and Gasser, 2007; Kind and van Steensel, 2010).

Here, we report the first systematic screen for factors required for the perinuclear sequestration of heterochromatin within a multicellular organism. Using a repetitive GFP-expressing transgene as a model for heterochromatin, we performed a genome-wide RNAi screen for both derepression and detachment. The only targets that compromised both encoded S-adenosylmethionine synthetases (Figure 2). This prompted us to carry out a systematic survey of putative HMTs, from which we identified two enzymes, MET-2 and SET-25, that mediate anchoring by methylation of histone H3K9 (Figure 3). In mutants lacking only one of the two HMTs, repetitive gene arrays remained perinuclear (Figure 3), whereas loss of both removed all H3K9me and eliminated array anchoring.

The only histone residue for which we scored reduced methylation in *met-2* and *set-25* mutants is H3K9. However, we do not exclude that it has other nonhistone substrates. The loss of HMTs that modify residues other than H3K9 did not affect array anchoring. We tested conditions that eliminated H3K27me3 (Figure S2C, *mes-2*; Bender et al., 2004), as well as H3K36me2/3 (Table S2, *mes-4 met-1*; Furuhashi et al., 2010), yet arrays remained anchored. Thus, we conclude that H3K9 methylation is a molecular signal for chromatin positioning at the NE and rule out a requirement for other histone H3 methyl marks in this process.

Despite strong correlations between peripheral localization and transcriptional inactivity, the two are not strictly linked in worms or in mammals (Meister et al., 2010; Peric-Hupkes et al., 2010). Indeed, we show that expression from the *baf-1* promoter on the GFP-LacI array is not sufficient for detachment. In the *set-25* single mutant, arrays were devoid of H3K9me3 and strongly derepressed, but due to the MET-2 deposited H3K9me1 and H3K9me2 modifications they remained enriched at the NE (Figures 3B and S2A and S2B). Similarly, *mes-4* and *hpl-2* mutations, and loss of several other chromatin factors, provoked strong derepression without altering array position (Figures S2B and S2C; Table S2). We can therefore exclude that the release of chromatin from the nuclear periphery in the *set-25 met-2* double mutant is explained by changes in promoter activity.

H3K9 Methylation Correlates with Lamin-Associated Domains from Worms to Man

The role of SET-25 and MET-2 in tethering chromatin to the NE is not limited to transgene arrays. We have shown that the same is true for endogenous loci in the repeat-rich arms of *C. elegans* chromosomes. Thus, our study provides the first causal evidence for a role of H3K9 methylation in perinuclear chromatin anchoring. DamID studies showed that 80% of non-centromeric H3K9me2 domains overlap with LADs in mammals (Peric-Hupkes et al., 2010; Wen et al., 2009). The anchoring of mammalian LADs has not previously been shown to be H3K9 dependent, but this striking correlation makes it is likely that the function of H3K9me1/2 in perinuclear chromatin anchoring is conserved beyond worms.

We show that H3K9me provides a signal to position chromatin at the NE. But what recognizes the H3K9me mark? Using genetic null alleles, we show that none of the H3K9me binding factors previously characterized in *C. elegans* are involved: array anchoring was unaltered upon loss of the HP1 homologs HPL-1 or HPL-2, alone or together, even in cells lacking the MBT domain protein LIN-61 (Figure S2C). This indicates that a novel class of yet uncharacterized factors mediates the molecular link between the nuclear periphery and H3K9me. Given that we identify a two-step anchoring process in which either H3K9me1/2 or H3K9me3 can signal peripheral localization, we also expect redundancy among these H3K9me readers, requiring combinatorial RNAi and/or screens in sensitized backgrounds to allow their identification.

Additional Pathways Position Chromatin in an H3K9me-Independent Manner

Diminished H3K9 methylation levels or loss of *met-2* causes a reduction in brood-size, low-penetrance embryonic lethality, a high incidence of males, and the formation of ectopic vulvae in sensitized backgrounds (Andersen and Horvitz, 2007; Koester-Eiserfunke and Fischle, 2011 and data not shown). Nevertheless, most *set-25 met-2* double-mutant animals are viable and fertile even though they lack detectable H3K9 methylation. Given the strict conservation of perinuclear chromatin anchoring from yeast to man (Kind and van Steensel, 2010), it is perhaps surprising that loss of anchoring is compatible with worm development. We note, however, that although the amplitude of LMN-1-DamID on chromosome arms was strongly reduced in the *met-2 set-25* mutant, chromosome arms retained slightly higher LMN-1-DamID signals than did chromosome centers (Figure 5). We also found that arrays become peripheral even in the absence of H3K9me upon cell differentiation (Figures S2F and S3). Thus, although we demonstrate a clear role for H3K9 methylation in perinuclear anchoring of chromatin in *C. elegans* embryos, partially redundant pathways of chromatin anchoring may ensure normal worm development even in the absence of H3K9 methylation.

A Conserved Two-Step Model for Generating H3K9me3-Containing Heterochromatic Foci

The establishment of H3K9me3 at mammalian centromeres has been proposed to occur in a step-wise manner by at least two enzymes (Loyola et al., 2006; Loyola et al., 2009; Peters et al., 2001). The methylation specificities of MET-2 and SET-25 argue for a similar step-wise methylation of H3K9 on perinuclear heterochromatin. Moreover, a step-wise mechanism is supported by the distinct subcellular localizations of the two enzymes. H3K9me1/2 is deposited by MET-2, which largely resides in the cytoplasm (Figure 6A). Similarly, SETDB1, the mammalian homolog of MET-2 (Loyola et al., 2006), and the two redundant mouse enzymes PRDM3 and PRDM16 (Pinheiro, et al., 2012, this issue of *Cell*) are abundant in the cytoplasm and mediate H3K9me1. Indeed, one-third of nonnucleosomal H3 carries K9me1 in mammals (Loyola et al., 2006).

We propose that after its nuclear import and incorporation into nucleosomes, H3K9me1/2 serves as a substrate for trimethylation by SET-25 (Figures 6B and 7). Given the enrichment of SET-25 in perinuclear foci, this latter step may occur preferentially at the nuclear periphery. The ability of H3K9me1/2 to mediate association with the nuclear envelope thus would promote trimethylation and repression. In mammalian cells

lacking both Suv39h isozymes, centromeres are devoid of H3K9me3, yet they remain clustered. A proposed explanation was that H3K9me1, which accumulates on centromeres in *suv39h1/2* double mutants (Peters et al., 2001), compensates for me3. Here, we show that this model holds for peripheral heterochromatin in *C. elegans*: arrays remained peripherally enriched in the absence of H3K9me3, but were entirely released in the set-*25 met-2* double mutant, which lacks all H3K9 methylation.

It has so far not been possible to deplete H3K9me1 completely from mammalian centromeres. However, recent evidence suggests that this can be achieved by simultaneous downregulation of the two H3K9-specific monomethyltransferases, PRDM3 and PRDM16 (Pinheiro et al., 2012, this issue of *Cell*). Analogous to our data implicating H3K9me1/2 in chromatin positioning, loss of H3K9me1 in mice provokes dispersion of centromeric foci and transcription of major satellite (Pinheiro et al., 2012, this issue of *Cell*).

A Self-Reinforcing Mechanism to Sequester Silent Chromatin at the Nuclear Periphery

Several HMTs are recruited to chromatin by the marks they deposit. It is generally assumed that this triggers the modification of neighboring nucleosomes and results in spreading of the chromatin mark (Bannister et al., 2001; Lachner et al., 2001). Evidence for such a mechanism exists for the propagation of H3K27me3 by PRC2 (Hansen et al., 2008), for the spreading of H3K9me3 in fission yeast by Clr4 (Zhang et al., 2008), and for the maintenance of H3K9me3 at centromeric repeats in mammals by Suv39 (Bannister et al., 2001; Lachner et al., 2001). In this sense, SET-25 fits the paradigm because it becomes enriched in foci that colocalize with H3K9me3. However, in contrast to Suv39h1/2, which are recruited to methylated H3K9 via HP1 (Bannister et al., 2001; Lachner et al., 2001), localization of SET-25 to perinuclear foci is independent of the two worm HP1 homologs (Figure S6). Moreover, SET-25 has little or no sequence homology to Suv39h outside its SET domain and lacks an identifiable Chromodomain. Future work will determine whether SET-25 binds directly to H3K9me3 or whether it is recruited by another nonhistone protein.

If H3K9 methylation is the trigger for perinuclear anchoring, the formation of heterochromatin itself should be able to drive its spatial separation from active chromatin domains. Because SET-25 associates with H3K9me3, the spatial separation of euchromatin and heterochromatin generates an unequal subnuclear distribution of the HMT that deposits the repressive H3K9me3 mark. Its perinuclear sequestration, in turn, has the potential to render the nuclear periphery a favorable zone for H3K9 trimethylation. This could act as a self-reinforcing silencing mechanism that ensures a robust spatial separation of active and inactive chromatin domains (Figure 7).

In conclusion, the histone modification and deposition pathway documented here suggests a means for the autonomous assembly of a subnuclear compartment that supports efficient heterochromatin formation. The many analogies to mammalian silencing suggest that the principles identified here have cross-species relevance.

EXPERIMENTAL PROCEDURES

Molecular Biology and Transgenic Strains

All plasmids, except plasmids for DamID constructs, were generated by MultiSite Gateway cloning (Invitrogen). The C645A mutation in *set-25* was introduced by site-directed mutagenesis. Strains used in this study are listed in Table S3. DamID strains were backcrossed twice, the *set-25(n5021)* and *met-2(n4256)* alleles five times to wild-type strains. Worms were grown at 22.5°C, except for the zoning assays in *lin-61 hpl-2* mutants (25°C) and for DamID (20°C).

RNAi

For individual assays, RNAi was performed by feeding on plates (Timmons et al., 2001). The RNAi screen was done in liquid cultures (adapted from Lehner et al., 2006, see Extended Experimental Procedures). An *EcoRV* fragment containing 25 bp identical to GFP-LacI was removed from vector L4440 (Fire vector library) and used as mock RNAi control. A strain supplemented with an additional copy of a *lacO* free *baf-1::GFP-lacI* transgene was used to enhance the GFP signal for *gwIs4* visualization.

Immunofluorescence and Fluorescence In Situ Hybridization

Immunofluorescence (IF) was carried out as previously described by freeze-cracking and brief fixation in 1% paraformaldehyde followed by short post-fixation in methanol (Meister et al., 2010). For quantitative histone IF and antibodies used see Extended Experimental Procedures.

Fluorescent probes were made by nick-translation using fluorescent dUTP-Atto647N (Jena Bioscience) and fosmid WRM0637cA03 as a template. For FISH, embryos were fixed in methanol (−20°C, 2′) followed by 4% paraformaldehyde (4°C, 10') after freeze-cracking. Embryos were permeabilized in PBS-Triton X-100 (0.5%) and treated briefly with 0.1M HCl and RNase. FISH probe and sample were denatured at 72°C and hybridized in 50% formamide/2X SSC for 3 days at 37°C, followed by three low- and two high-stringency washes (2X SSC, 37°C / 0.2X SSC, 55°C).

Microscopy

Microscopy was carried out on a spinning disc confocal microscope (Visitron, Puchheim), as previously described (Meister et al., 2010). Deconvolution (Huygens Pro) was applied to Figures 5, 6, S5, and S6. 3D reconstructions were generated by using Imaris (Bitplane). Quantitation of array distribution on focal stacks of images using the ImageJ plugin PointPicker (http://bigwww.epfl.ch/thevenaz/pointpicker/) was performed as previously described (Meister et al., 2010). For radial quantitation of H3K9me, 200 nm spaced image stacks were acquired and processed by deconvolution. Using >120 independent manually selected line profiles (5 pixels wide) at the central nuclear plane, lines were extended laterally by 12.5% of the nuclear diameter, and signal intensities were extracted and pooled into 100 bins. Individual profiles were normalized, averaged, and plotted by using R.

Isolation of Histones and Mass Spectrometry

Early embryos were obtained by bleaching from synchronized young adults grown for 53 to 58 hr after L1 stage at 22.5°C. H3 was isolated for mass spectroscopy as described in Extended Experimental Procedures. Free and monomethylated amino groups were chemically modified with propionic anhydride prior trypsin digestion (Peters et al., 2003). After elution from gel the differently methylated peptides were quantified by LC-MRM on an AB SCIEX 4000 QTRAP, and peak area ratios were normalized to wild-type and histone H3.

LMN-1-DamID

All DamID constructs were integrated as a single-copy on Chromosome II by MosSCI (Frøkjaer-Jensen et al., 2008). Details on strains, plasmids, DNA isolation, and computational analysis are in Extended Experimental Procedures.

ACCESSION NUMBERS

The GEO accession number for the DamID microarray raw data is GSE37226.

SUPPLEMENTAL INFORMATION

Supplemental Information includes Extended Experimental Procedures, six figures, and four tables and can be found with this article online at http://dx.doi.org/10.1016/j.cell.2012.06.051.

ACKNOWLEDGMENTS

We thank Y. Gruenbaum and T. Jenuwein for antibodies; M. Thomas, R. Arpagaus, R. Son, and T. Sakuragi for excellent technical assistance; I. Katic for help with injections; the *Caenorhabditis* Genetics Center; R. Horvitz, M. Tijsterman and F. Palladino for strains; D. Schübeler, A. Peters, and H. Ferreira for critical reading of the manuscript; and L. Hoerner for help with array hybridization. This work was supported by the European Union Network of Excellence "Epigenome", the Novartis Research Foundation, the "Fondation Suisse de recherche sur les maladies musculaires", the Spanish Ministry of Science and Innovation (BFU2010-15478 to P.A.), and EMBO (ASTF 478-2011 to C.G.A.).

Received: June 12, 2011
Revised: April 5, 2012
Accepted: June 26, 2012
Published: August 30, 2012

REFERENCES

Akhtar, A., and Gasser, S.M. (2007). The nuclear envelope and transcriptional control. Nat. Rev. Genet. *8*, 507–517.

Andersen, E.C., and Horvitz, H.R. (2007). Two *C. elegans* histone methyltransferases repress *lin-3* EGF transcription to inhibit vulval development. Development *134*, 2991–2999.

Azzaria, M., Goszczynski, B., Chung, M.A., Kalb, J.M., and McGhee, J.D. (1996). A fork head/HNF-3 homolog expressed in the pharynx and intestine of the *Caenorhabditis elegans* embryo. Dev. Biol. *178*, 289–303.

Bannister, A.J., Zegerman, P., Partridge, J.F., Miska, E.A., Thomas, J.O., Allshire, R.C., and Kouzarides, T. (2001). Selective recognition of methylated lysine 9 on histone H3 by the HP1 chromo domain. Nature *410*, 120–124.

Bender, L.B., Cao, R., Zhang, Y., and Strome, S. (2004). The MES-2/MES-3/MES-6 complex and regulation of histone H3 methylation in *C. elegans*. Curr. Biol. *14*, 1639–1643.

Bender, L.B., Suh, J., Carroll, C.R., Fong, Y., Fingerman, I.M., Briggs, S.D., Cao, R., Zhang, Y., Reinke, V., and Strome, S. (2006). MES-4: an autosome-associated histone methyltransferase that participates in silencing the X chromosomes in the *C. elegans* germ line. Development *133*, 3907–3917.

Bessler, J.B., Andersen, E.C., and Villeneuve, A.M. (2010). Differential localization and independent acquisition of the H3K9me2 and H3K9me3 chromatin modifications in the *Caenorhabditis elegans* adult germ line. PLoS Genet. *6*, e1000830.

Black, J.C., and Whetstine, J.R. (2011). Chromatin landscape: methylation beyond transcription. Epigenetics *6*, 9–15.

Capowski, E.E., Martin, P., Garvin, C., and Strome, S. (1991). Identification of grandchildless loci whose products are required for normal germ-line development in the nematode *Caenorhabditis elegans*. Genetics *129*, 1061–1072.

Dennis, G., Jr., Sherman, B.T., Hosack, D.A., Yang, J., Gao, W., Lane, H.C., and Lempicki, R.A. (2003). DAVID: Database for Annotation, Visualization, and Integrated Discovery. Genome Biol. *4*, 3.

Frøkjaer-Jensen, C., Davis, M.W., Hopkins, C.E., Newman, B.J., Thummel, J.M., Olesen, S.-P., Grunnet, M., and Jorgensen, E.M. (2008). Single-copy insertion of transgenes in *Caenorhabditis elegans*. Nat. Genet. *40*, 1375–1383.

Furuhashi, H., Takasaki, T., Rechtsteiner, A., Li, T., Kimura, H., Checchi, P.M., Strome, S., and Kelly, W.G. (2010). Trans-generational epigenetic regulation of *C. elegans* primordial germ cells. Epigenetics Chromatin *3*, 15.

Goldman, R.D., Gruenbaum, Y., Moir, R.D., Shumaker, D.K., and Spann, T.P. (2002). Nuclear lamins: building blocks of nuclear architecture. Genes Dev. *16*, 533–547.

Guelen, L., Pagie, L., Brasset, E., Meuleman, W., Faza, M.B., Talhout, W., Eussen, B.H., de Klein, A., Wessels, L., de Laat, W., and van Steensel, B. (2008). Domain organization of human chromosomes revealed by mapping of nuclear lamina interactions. Nature *453*, 948–951.

Hansen, K.H., Bracken, A.P., Pasini, D., Dietrich, N., Gehani, S.S., Monrad, A., Rappsilber, J., Lerdrup, M., and Helin, K. (2008). A model for transmission of the H3K27me3 epigenetic mark. Nat. Cell Biol. *10*, 1291–1300.

Hsieh, J., and Fire, A. (2000). Recognition and silencing of repeated DNA. Annu. Rev. Genet. *34*, 187–204.

Ikegami, K., Egelhofer, T.A., Strome, S., and Lieb, J.D. (2010). *Caenorhabditis elegans* chromosome arms are anchored to the nuclear membrane via discontinuous association with LEM-2. Genome Biol. *11*, R120.

Kamath, R.S., Fraser, A.G., Dong, Y., Poulin, G., Durbin, R., Gotta, M., Kanapin, A., Le Bot, N., Moreno, S., Sohrmann, M., et al. (2003). Systematic functional analysis of the *Caenorhabditis elegans* genome using RNAi. Nature *421*, 231–237.

Kind, J., and van Steensel, B. (2010). Genome-nuclear lamina interactions and gene regulation. Curr. Opin. Cell Biol. *22*, 320–325.

Koester-Eiserfunke, N., and Fischle, W. (2011). H3K9me2/3 binding of the MBT domain protein LIN-61 is essential for *Caenorhabditis elegans* vulva development. PLoS Genet. *7*, e1002017.

Lachner, M., O'Carroll, D., Rea, S., Mechtler, K., and Jenuwein, T. (2001). Methylation of histone H3 lysine 9 creates a binding site for HP1 proteins. Nature *410*, 116–120.

Lehner, B., Tischler, J., and Fraser, A.G. (2006). RNAi screens in *Caenorhabditis elegans* in a 96-well liquid format and their application to the systematic identification of genetic interactions. Nat. Protoc. *1*, 1617–1620.

Liu, T., Rechtsteiner, A., Egelhofer, T.A., Vielle, A., Latorre, I., Cheung, M.-S., Ercan, S., Ikegami, K., Jensen, M., Kolasinska-Zwierz, P., et al. (2011). Broad chromosomal domains of histone modification patterns in *C. elegans*. Genome Res. *21*, 227–236.

Loyola, A., Bonaldi, T., Roche, D., Imhof, A., and Almouzni, G. (2006). PTMs on H3 variants before chromatin assembly potentiate their final epigenetic state. Mol. Cell *24*, 309–316.

Loyola, A., Tagami, H., Bonaldi, T., Roche, D., Quivy, J.P., Imhof, A., Nakatani, Y., Dent, S.Y.R., and Almouzni, G. (2009). The HP1α-CAF1-SetDB1-containing complex provides H3K9me1 for Suv39-mediated K9me3 in pericentric heterochromatin. EMBO Rep. *10*, 769–775.

Luo, L., Gassman, K.L., Petell, L.M., Wilson, C.L., Bewersdorf, J., and Shopland, L.S. (2009). The nuclear periphery of embryonic stem cells is a transcriptionally permissive and repressive compartment. J. Cell Sci. *122*, 3729–3737.

Maison, C., and Almouzni, G. (2004). HP1 and the dynamics of heterochromatin maintenance. Nat. Rev. Mol. Cell Biol. *5*, 296–304.

Margalit, A., Brachner, A., Gotzmann, J., Foisner, R., and Gruenbaum, Y. (2007). Barrier-to-autointegration factor—a BAFfling little protein. Trends Cell Biol. *17*, 202–208.

Martin, D.I.K., and Whitelaw, E. (1996). The vagaries of variegating transgenes. Bioessays *18*, 919–923.

Mattout, A., Pike, B.L., Towbin, B.D., Bank, E.M., Gonzalez-Sandoval, A., Stadler, M.B., Meister, P., Gruenbaum, Y., and Gasser, S.M. (2011). An EDMD mutation in *C. elegans* lamin blocks muscle-specific gene relocation and compromises muscle integrity. Curr. Biol. *21*, 1603–1614.

Meister, P., Towbin, B.D., Pike, B.L., Ponti, A., and Gasser, S.M. (2010). The spatial dynamics of tissue-specific promoters during *C. elegans* development. Genes Dev. *24*, 766–782.

Peric-Hupkes, D., Meuleman, W., Pagie, L., Bruggeman, S.W.M., Solovei, I., Brugman, W., Gräf, S., Flicek, P., Kerkhoven, R.M., van Lohuizen, M., et al. (2010). Molecular maps of the reorganization of genome-nuclear lamina interactions during differentiation. Mol. Cell *38*, 603–613.

Peters, A.H.F.M., O'Carroll, D., Scherthan, H., Mechtler, K., Sauer, S., Schöfer, C., Weipoltshammer, K., Pagani, M., Lachner, M., Kohlmaier, A., et al. (2001). Loss of the Suv39h histone methyltransferases impairs mammalian heterochromatin and genome stability. Cell *107*, 323–337.

Peters, A.H.F.M., Kubicek, S., Mechtler, K., O'Sullivan, R.J., Derijck, A.A.H.A., Perez-Burgos, L., Kohlmaier, A., Opravil, S., Tachibana, M., Shinkai, Y., et al. (2003). Partitioning and plasticity of repressive histone methylation states in mammalian chromatin. Mol. Cell *12*, 1577–1589.

Pickersgill, H., Kalverda, B., de Wit, E., Talhout, W., Fornerod, M., and van Steensel, B. (2006). Characterization of the *Drosophila melanogaster* genome at the nuclear lamina. Nat. Genet. *38*, 1005–1014.

Pinheiro, I., Margueron, R., Shukeir, N., Eisold, M., Fritzsch, C., Richter, F.M., Mittler, G., Genoud, C., Goyama, S., Kurokawa, M., et al. (2012). Prdm3 and Prdm16 are H3K9me1 Methyltransferases Required for Mammalian Heterochromatin Integrity. Cell *150*, this issue, 948–960.

Rea, S., Eisenhaber, F., O'Carroll, D., Strahl, B.D., Sun, Z.-W., Schmid, M., Opravil, S., Mechtler, K., Ponting, C.P., Allis, C.D., and Jenuwein, T. (2000). Regulation of chromatin structure by site-specific histone H3 methyltransferases. Nature *406*, 593–599.

Sassi, H.E., Renihan, S., Spence, A.M., and Cooperstock, R.L. (2005). Gene CATCHR—gene cloning and tagging for *Caenorhabditis elegans* using yeast homologous recombination: a novel approach for the analysis of gene expression. Nucleic Acids Res. *33*, e163.

Schott, S., Coustham, V., Simonet, T., Bedet, C., and Palladino, F. (2006). Unique and redundant functions of *C. elegans* HP1 proteins in post-embryonic development. Dev. Biol. *298*, 176–187.

Shevelyov, Y.Y., Lavrov, S.A., Mikhaylova, L.M., Nurminsky, I.D., Kulathinal, R.J., Egorova, K.S., Rozovsky, Y.M., and Nurminsky, D.I. (2009). The B-type lamin is required for somatic repression of testis-specific gene clusters. Proc. Natl. Acad. Sci. USA *106*, 3282–3287.

Tachibana, M., Sugimoto, K., Nozaki, M., Ueda, J., Ohta, T., Ohki, M., Fukuda, M., Takeda, N., Niida, H., Kato, H., and Shinkai, Y. (2002). G9a histone methyltransferase plays a dominant role in euchromatic histone H3 lysine 9 methylation and is essential for early embryogenesis. Genes Dev. *16*, 1779–1791.

Timmons, L., Court, D.L., and Fire, A. (2001). Ingestion of bacterially expressed dsRNAs can produce specific and potent genetic interference in *Caenorhabditis elegans*. Gene *263*, 103–112.

Wen, B., Wu, H., Shinkai, Y., Irizarry, R.A., and Feinberg, A.P. (2009). Large histone H3 lysine 9 dimethylated chromatin blocks distinguish differentiated from embryonic stem cells. Nat. Genet. *41*, 246–250.

Ye, Q., and Worman, H.J. (1996). Interaction between an integral protein of the nuclear envelope inner membrane and human chromodomain proteins homologous to *Drosophila* HP1. J. Biol. Chem. *271*, 14653–14656.

Yuzyuk, T., Fakhouri, T.H.I., Kiefer, J., and Mango, S.E. (2009). The polycomb complex protein *mes-2*/E(z) promotes the transition from developmental plasticity to differentiation in *C. elegans* embryos. Dev. Cell *16*, 699–710.

Zhang, K., Mosch, K., Fischle, W., and Grewal, S.I.S. (2008). Roles of the Clr4 methyltransferase complex in nucleation, spreading and maintenance of heterochromatin. Nat. Struct. Mol. Biol. *15*, 381–388.